Title: Assessment of the morphology, microstructure, stereometric and tribological properties of Al2O3 surface layers produced electrolytically with the alternating current method in the presence of molybdenum disulfide

Author: Adrian Kędra, Mariusz Koziarz, Tomasz Kmita, Dariusz Bochenek, Sławomir Kaptacz, Adrian Barylski, Joanna Korzekwa

Citation style: Kędra Adrian, Koziarz Mariusz, Kmita Tomasz, Bochenek Dariusz, Kaptacz Sławomir, Barylski Adrian, Korzekwa Joanna. (2021). Assessment of the morphology, microstructure, stereometric and tribological properties of Al2O3 surface layers produced electrolytically with the alternating current method in the presence of molybdenum disulfide. "Tribology Online" (2021), Vol. 16, iss. 4, art. no. 21147, s. 223-235. DOI: 10.2474/trol.16.223

Tribology Online

Japanese Society of Tribologists
http://www.tribology.jp/trol/

Vol. 16, No. 4 (2021) 223-235.
ISSN 1881-2198
DOI 10.2474/trol.16.223

Article

Assessment of the Morphology, Microstructure, Stereometric and Tribological Properties of Al_2O_3 Surface Layers Produced Electrolytically with the Alternating Current Method in the Presence of Molybdenum Disulfide

Adrian Kędra, Mariusz Koziarz, Tomasz Kmita, Dariusz Bochenek, Sławomir Kaptacz, Adrian Barylski and Joanna Korzekwa*

[1)] Faculty of Science and Technology, Institute of Materials Engineering, University of Silesia in Katowice, 75 Pułku Piechoty 1a, 41–500 Chorzów, Poland

*Corresponding author: Joanna Korzekwa (joanna.korzekwa@us.edu.pl)

Manuscript received 07 July 2021; accepted 18 September 2021; published 31 October 2021

Abstract

Dry friction tests were performed using a pin-on-plate tribological tester. In this study, Al_2O_3 and Al_2O_3 with MoS_2 admixture plate with PEEK/BG pin. Plate surfaces were created using the constant current method and the non-periodic alternating current method. The dimension of Al_2O_3 fibers walls were calculate based on SEM micrographs. SGP measurements of the oxide layers were made by a Taylor Hobson Talysurf 2D pin profilometer. It was found that the gradient structure favors the reduction of the friction coefficient and weight loss of PEEK/BG in the tested friction pairs, and the method of gradually reducing non-periodic alternating current allowed to obtain a more homogeneous microstructure of aluminum oxide. The use of high current densities at the beginning of the process leads to the production of non-gradient coatings characterized by higher SGP amplitude parameters. This property translates directly into higher wear of the sliding PEEK/BG material and higher values of the friction coefficients of the tribological pairs thus obtained. The research also identified a strong correlation between the friction coefficient μ and surface topography parameters before the tribological cooperation of PEEK/BG pairs - Al_2O_3 oxide coating.

Keywords

coatings, oxide layer, anodizing, stereometry, tribology

1 Introduction

Hard anodizing is one of the methods of coating a metal surface with Al_2O_3 aluminum oxide. The direct current method (DC) with controlled current density maintains a constant value of the current intensity throughout the layer formation process. The voltage during anodizing initially increases drastically due to the spontaneously formed thin aluminum oxide coating. This phenomenon is related to the resistance exerted by the layer to the flowing current. Then, after breaking through the barrier layer, the voltage drops immediately and slowly increases over time. Both reactions are exothermic, and the properties of the layer formed in such a process depend mainly on the current strength, chemical composition, and temperature of the electrolyte and the chemical composition of the substrate, e.g., aluminum alloy [1–3].

The constant voltage method consists of maintaining a constant voltage in the entire range of obtaining the layer. Initially, the current density drops sharply to a sharp minimum and slowly increases over time. This method of obtaining the Al_2O_3 layer was used, among others, by [4] where it was proved that the purity and reasonable temperature of annealing of the aluminum substrate are a fundamental process allowing to obtain a highly ordered system of nanopores on the anodic aluminum oxide layer. Furthermore, the authors [5], who also obtained Al_2O_3 layers using the constant voltage method, suggest that electrode separation should also be taken into account by scientists and technologists dealing with these areas, both as a control and design parameter of anodizing process.

As mentioned, hard anodizing is an exothermic process associated with the release of Joule heat [6]; therefore, temperature control and the requirement to cool the electrolyte are essential. In addition, the application of high voltage during the fabrication of the coating can result in sparking between the coating and the electrolyte. This voltage can result in a local temperature rise affecting the heterogeneity of the coating [7].

The oxide layers can also be obtained by the alternating current (AC) method. The advantage of this method is the ability to create composite layers based on alumina. In the AC method, the current can be periodically alternating (pulsating

or alternating current) or non-periodic alternating current. The pulse method is based on applying an alternating current of a rectangular shape to the anode. This method has many advantages over DC anodizing. Thanks to the control of parameters such as pulse filling, vibration period, and current amplitude, we can control the system so that it does not require electrolyte cooling. Better homogeneity of the surface is achieved than classical methods, a greater layer thickness, and roughness and microhardness control [8–16].

It is well known that different surfaces reflect different tribological properties, the roughness having a significant influence on the level of friction under dry and lubricated conditions, conditions for the formation of a lubricant film, load capacity [17, 18]. An important part of the experimental research related to the industrial application is the measurement and evaluation of the geometric structure of the surface of machine elements and tools [19–22, 23]. The authors [24, 25] showed a new strategy for predicting friction and possible applications in engineering. When examining carbon alloys and carbon titanium alloys, it was found that the initial surface roughness has a significant impact on friction, wear process and wear activation energy [26]. The results of the ball and disk tests show the existence of a correlation between the parameters of the surface topography (in particular R_{sk} and R_{ku}) and the friction force [27, 28].

2 Experiment

The test specimens were made on the EN-AW 5251 aluminum alloy. In order to oxidize the selected part of the aluminum alloy, a significant part of the specimen was glued with distal classic two-component epoxy glue [29]. Figure 1 shows the procedure of the sample preparations. The oxidation process was applied to 5 cm^2 of the surface, which was used to study the microstructure of the layer. The electrolyte was an aqueous solution of sulfuric, phthalic, and oxalic acids with the addition of 30 grams of molybdenum disulfide powder per liter of electrolyte. Initially, the samples were digested in sodium hydroxide solution for about 30 minutes and then rinsed in distilled water for 5 minutes. The next step was to neutralize the KOH hydroxide in the nitric acid solution for 5 minutes and rinse again in distilled water. Due to the consistency of the electrolyte and the content of MoS_2, which is heavier than the acid solution and sinks to the bottom of the container, an insulated mechanical stirrer is inserted in the center, ensuring even distribution of MoS_2 powder in the electrolyte volume. Mixing during the surface production was changed to avoid layers of varying thickness and for better homogenization. To evaluate the resulting structure under similar conditions, the current density for each sample produced was so good over time as to obtain an average of 3 A/dm^2 with an anodizing time of approximately 52 min. The reference sample was made using the constant current method at the temperature of 30°C. Table 1 shows the names and descriptions of the studied samples. The next step was to perform samples with a step-change in current over time by the non-periodic alternating current method. The flowing current was gradually increased (Figs. 2 a and c) or reduced (Figs. 2 b and d) to maintain an average current intensity of 3 A /dm^2 over time for each sample and compare them to referring sample named A3.

3 Methodological bases

Micrographs of the structure and morphology of the formed surface oxide layers were taken using a JEOL JSM-7100 TTL LV field emission scanning electron microscope (Jeol Ltd., Tokyo, Japan). The samples for the measurements were sputtered with gold. To calculate the dimension of Al_2O_3 fibers walls, ImageJ software 1.50i (LOCI, University of Wisconsin, Madison, US) was used. A DC GPR-25H30D GW Instek (IET labs, Inc, NY, US) power supply was used for the hard anodizing process. The thickness of the oxide layers was measured with a Dualscope MP40 by Fischer (Helmut Fischer GmbH+Co.KG, Sindelfingen, Germany), using the eddy current method. The microhardness HV 0,1 was tested on a Wolpert Instruments model 401 MVD device (Wolpert Wilson, Worcester, MA, USA) with a Vickers diamond indenter with a cone angle of 138° at a load of 100 gf (0.98 N). The holding time under full load was 10s. The result

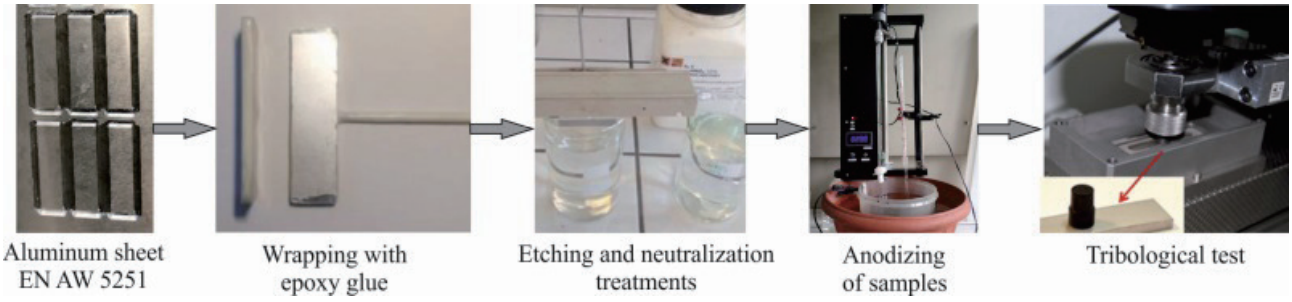

Fig. 1 A sample preparation scheme

Table 1 Names and descriptions of studied samples

Name of samples	Method of anodizing	Current density [A/dm^2]	MoS_2 concentration [g/l]
A3	DC	3	0
AMo2_4	AC	2-4	30
AMo4_2	AC	4-2	30
AMo1-5	AC	1-5	30
AMo5_1	AC	5-1	30

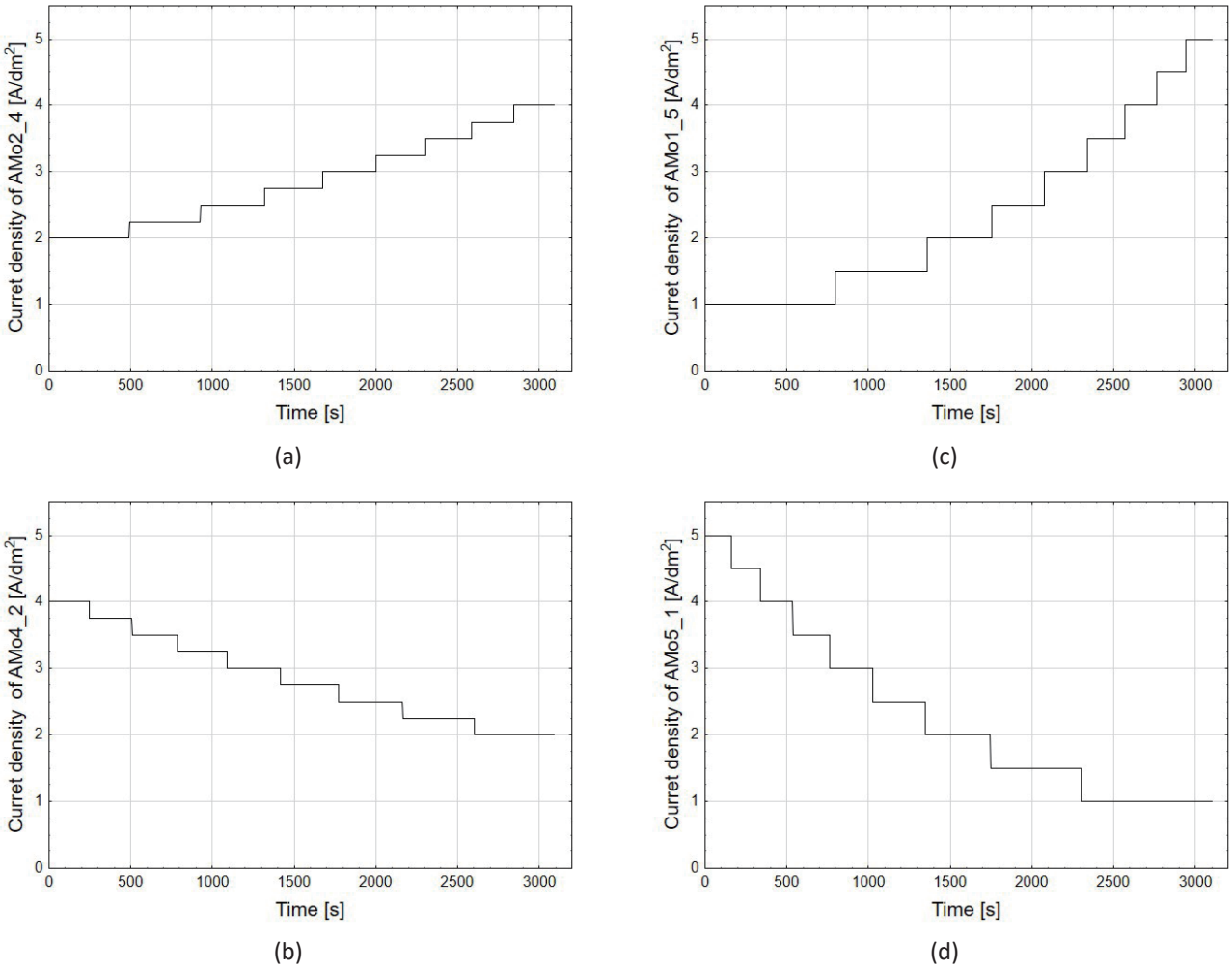

Fig. 2 The course of the current intensity over time, while maintaining an average charge of 3 A/dm² of (a) AMo2_4, (b) AMo4_2, (c) AMo1_5, (d) AMo5_1

of each measurement was the average of 5 Vickers indentations made on the surface of the coatings.

Tribological measurements were performed on a T17 tester (Łukasiewicz Research Network - The Institute for Sustainable Technologies, Radom, Poland), pin-on-plate in reciprocating motion, at room temperature, at the humidity of 50% ± 10%, at the average sliding speed velocity of 0.2 m/s and a running frequency of 2.5 Hz in dry friction conditions. The tribological test was conducted for the sliding distance of 15 km. The sliding trace was 40 mm. A commercial PEEK/BG (carbon fiber and polytetrafluoroethylene -PTFE) plastic pin of a diameter of 9 mm was used as a counter-body. The average value of the coefficient of friction was calculated when the coefficient of friction change curve reached the rectilinear range. The wear quantity of the polymeric pin was studied using a WPA-60G (Radwag) analytical scale with the accuracy of ± 0.1 mg before and after each friction cycle.

Geometric parameters defining the structure were called SGP (Surface Geometric Parameter). SGP measurements of the oxide layers were made by a Taylor Hobson Talysurf 2D pin profilometer (Taylor Hobson, Leicester, UK) with an accuracy of ± 2%. The results of the parameters were developed by using the TalyMap Universal 3D software. To characterize the surface stereometry, vertical parameters were selected, i.e., S_q, S_{sk}, S_{ku}, S_p, S_v, S_z, and parameters based on the Abbot-Firestone curve, i.e., S_k, S_{pk}, S_{vk}. S_q is the standard deviation of the surface amplitudes. This parameter is characterized by averaged surface amplitude; its sensitivity to measurement errors is low. S_{sk} (skewness of the assessed surface topography) and S_{ku} (kurtosis of the surface topography) describe the shape of the ordinate distribution. The combination of skew and kurtosis allows the identification of steep slopes and deep valleys on the surface. The functional parameters S_{pk} (reduced peak height), S_k (core depth), and S_{vk} (reduced valley depth) characterize the heights of three parts of the profile: peak, core, and valley, respectively. They are obtained based on the material indicator curve. These parameters are important from a tribological point of view [30].

4 Results and discussion

4.1 Characterizations of the coatings

The average values of the oxide layer thickness were in the range of 35, 64 – 51 μm (Fig. 3).

The highest value of thickness was noticed for reference sample A3. Higher values of thickness characterized layers obtained at a smaller span of current intensity AMo2_4 and AMo4_2 compare to the layers obtained at the broader span of current intensity AMo1_5 and AMo5_1. The more significant

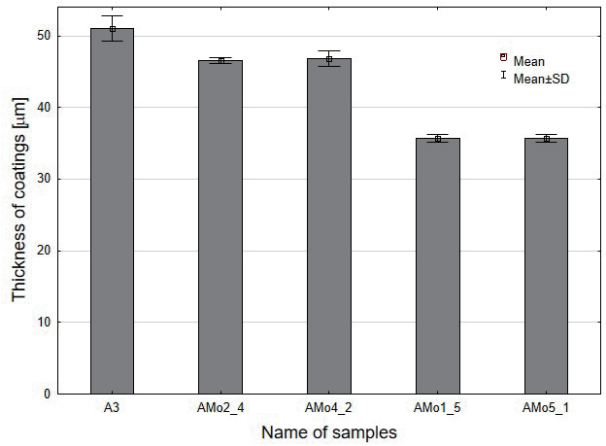

Fig. 3 The thickness of the oxide layer on aluminum samples

difference in the applied amperage resulted in a thinner layer of aluminum oxide.

Figure 4 shows the microhardness charts for the obtained samples. The lowest microhardness values were obtained for the AMo2_4 and AMo1_5 samples. However, it is difficult to talk about significant differences taking into account the standard deviation.

The SEM images in Fig. 5 present the example of changes in the dimension of Al_2O_3 fibers walls depending on the distance from aluminum alloy substrate for sample AMo1_5.

Measurements of fiber wall dimensions were done manually in ImageJ. Figure 6 shows a scheme for measuring the size of the wall of Al_2O_3 fiber.

Aluminum oxide nanofiber seen across SEM image is the wall of a single cell of aluminum oxide with a certain thickness. The thickness of this wall is the variable "d" described in Fig. 6. "d" is the dimension of the perpendicular cross-section of the fiber of aluminum oxide. For calculating

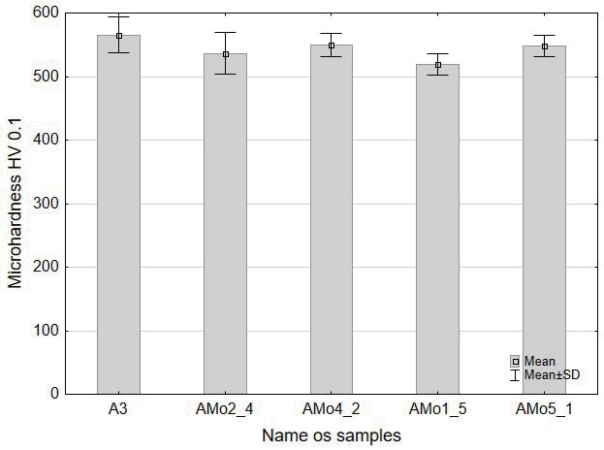

Fig. 4 The microhardness charts for the obtained samples

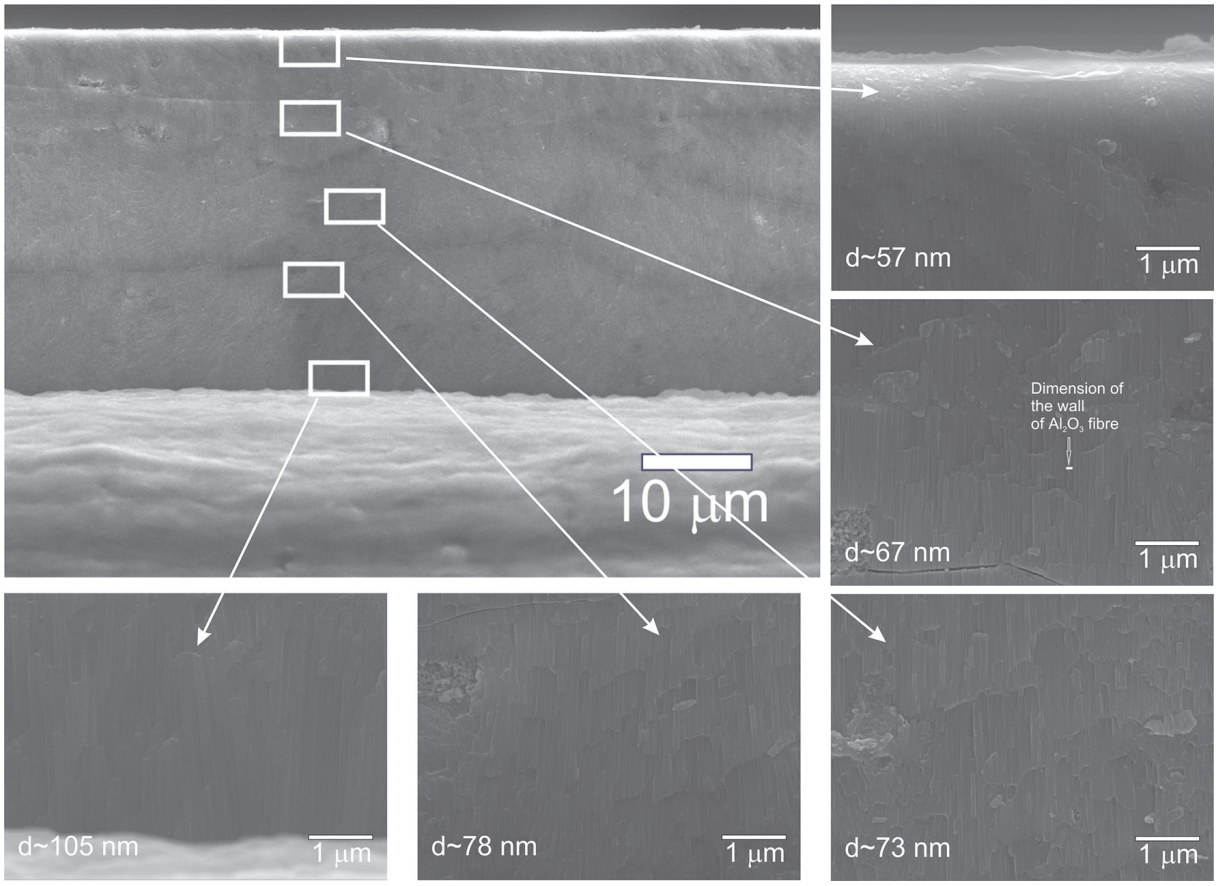

Fig. 5 The SEM pictures example (AMo1_5 sample) of changes in the dimension of Al_2O_3 fibers walls depending on the distance from aluminum alloy substrate

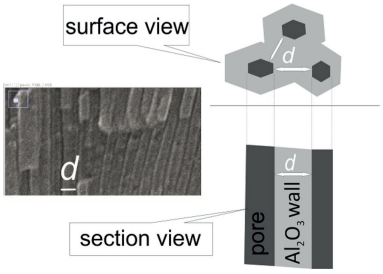

Fig. 6 A scheme for measuring the size of the Al_2O_3 fiber wall

the "d" dimension of the "nanofibers", 5 to 7 photos were taken along the cross-section of the coating. On each of the photos, the thickness of 25 adjacent aluminum oxide nanofibers was measured. The dark areas in the SEM image in Fig. 6 are nanopores. The walls of the nanofiber in the SEM image in Fig. 6 are seen as one bright line. In fact, they are the interconnected walls of the adjacent cells of the Al_2O_3 structure. Based on the measurements carried out in Fig. 5, an analysis of the fiber dimension was carried out depending on the technological conditions. The obtained results indicate that the application of the non-periodic alternating current method results in the occurrence of local changes in the nanostructure of the anodic Al_2O_3 fibers.

For the samples obtained during the stepwise increasing anodizing current (Figs. 7 b and c), the dimensions of the walls of the aluminum oxide fibers at the substrate were over 100 nm. For samples AMo2_4 and AMo1_5 obtained in this way, a tendency to decrease the size of the aluminum oxide fiber walls with the increase of the layer from the substrate can be observed. Similar behavior was recorded for the reference sample A3. Along with the decrease in the size of the walls of the aluminum oxide fibers, an increase in the number of fibers can also be observed (Fig. 5). The performed measurements showed that the high initial current and its gradual reduction over time during the preparation of samples AMo4_2 and AMo5_1 led to a more uniform size of the aluminum oxide fiber walls across the width of the layer (Figs. 7 d and f). The base sample A3 and samples AMo2_4 and AMo1_5 are characterized by a gradient structure, which is confirmed by the linear regression coefficients of a straight line fitted to the obtained results (Figs. 7 a, b, c). In AMo4_2 and AMo5_1, the linear regression coefficients are ~ -1.8 and ~ 0.4, respectively, which indicates a constant value of the aluminum oxide fiber wall size in the layer (Figs. 7 d and e). The process of dissolving the formed oxide by the acid present in the electrolyte leads to a gradient structure of layers obtained electrolytically on aluminum (the acid has longer contact with the outer area of the coating). Applying a higher current density at the beginning of the process increases the thickness of the fibers and decreases the porosity. Applying a higher current at the beginning of the electrolytic process may thus counteract the natural process of creating a gradient structure change. When lower current is used, we enhance the natural effect of acid dissolving the structure.

4.2 Tribological properties of the coatings

Figure 8 a shows PEEK/BG material temperature changes depending on the friction path during the tribological test. For all samples, there was a tendency to increase the temperature of PEEK/BG plastic. This increase is related to the intense abrasion of unevenness on the surface of the more plastic PEEK/BG sample due to the hard surface roughness of the Al_2O_3 layer. In tribology, this period is called the running-in stage, and in the case of the tested layers, the maximum temperature associated with this stage occurs for the first 6 km of the friction path. Then, a slight decrease in the temperature value can be noticed. After approximately 11 km of the road, a rectilinear diagram should be interpreted as the proper period of tribological cooperation. The area of the rectilinear graph of temperature dependence on the friction path generally coincides with the stabilized course of the friction coefficient value from the friction path (Fig. 8 b). This range becomes the basis for calculating the average coefficient of friction for each tribological pair. The value of the average coefficient of friction is shown in Fig. 9 a. On the other hand, Fig. 9 b shows the weight loss of PEEK/BG material after tribological cooperation. The lowest mean value of the friction coefficient was obtained for the layer AMo1_5, which was $\mu = 0.136 \pm 0.002$. In the tribological combination of this layer with the polymer pre-sample, the lowest PEEK/BG material consumption was also noted, amounting to 0.0009 g. The highest values of the friction coefficient $\mu = 0.174 \pm 0.006$ and $\mu = 0.169 \pm 0.003$ were found in the layers AMo5_1 and AMo4_2, respectively. Also, the weight loss values of PEEK/BG material with these layers were the highest and amounted to 0.00459 g and 0.0026 g, respectively, for the layers AMo4_2 and AMo5_1, respectively.

4.3 Relationship between the surface parameters and tribological properties of the coatings

In Figs. 10-14, the isometric images of samples before (a) and after (b) friction test were presented.

Figure 15 shows the surface photos of the tested samples after the tribological test.

Table 2 shows the stereometric parameters of the surfaces of the surface layers before and after the tribological test. Figure 16 a shows the mean square deviation of the S_q profile, and Fig. 16 b shows the total depth of the S_t profile for individual surface layers before and after the tribological test. According to the results presented in Fig. 16 a, a decrease in the surface roughness value was observed after tribological cooperation for all tested layers, regardless of the electrolysis conditions. They were smoothing the surface after tribological cooperation is related to both the friction process and the transfer of the PEEK/BG material to the surface of the layer. The highest value of the S_q parameter, amounting to 1.37 μm, was recorded before the tribological cooperation for the AMo5_1 layer. The S_q parameter value characterized the other layers in the range of 0.672 - 0.809 μm. The S_q parameter, which reflects the nature of surface unevenness, is sensitive to single indentations and elevations. Parameter S_t, the total profile depth is the sum of the parameters S_p, i.e., the height of the highest elevation of the profile, and S_v, i.e., the depth of the lowest profile cavity. The highest values of the S_t parameter, amounting to 11.11 and 12.35 μm, were recorded, respectively, before the tribological cooperation for the layers AMo4_2 and AMo5_1. These layers were characterized by the highest friction coefficient and the loss of the PEEK/BG counter-sample. During the cooperation with the AMo5_1 layer, the highest temperature value of the PEEK/BG sub-sample was noticed (Fig. 8 a), and the highest friction coefficient for this tribological pair $\mu = 0.174 \pm 0.006$ (Fig. 6 a). 0.0026 g of PEEK/BG polymer (Fig. 9 b) was rubbed off. Also, cooperation with the AMo4_2 layer resulted in high PEEK/BG material consumption in the amount of 0.00459 g (Fig. 9 b), the coefficient of friction $\mu = 0.169 \pm 0.003$ (Fig. 9 a).

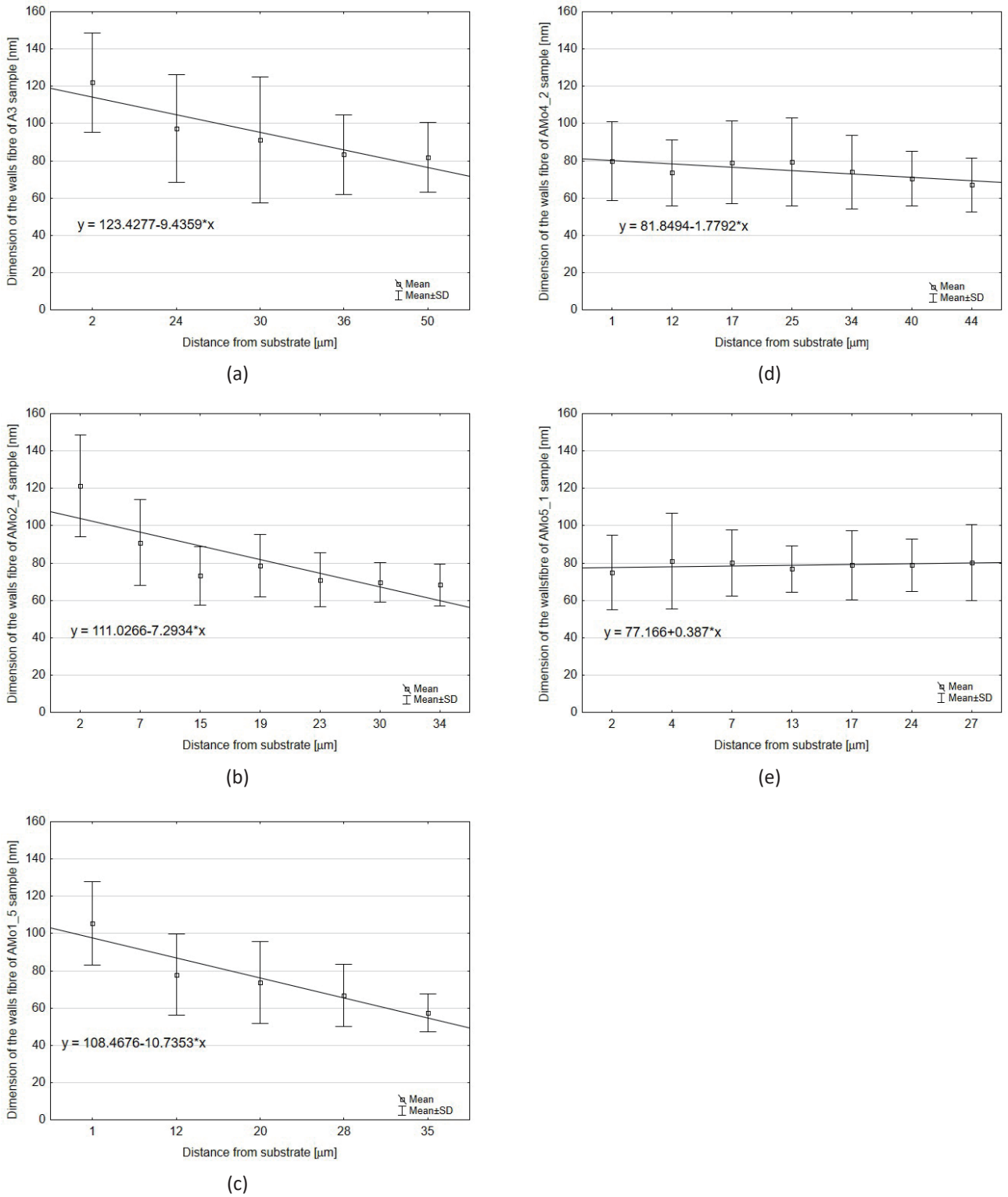

Fig. 7 Dimension of the walls of Al_2O_3 fibre of (a) A3, (b) AMo2_4, (c) Amo1_5, (d) AMo4_2, (e) AMo5_1 sample

The parameters S_{sk} and S_{ku} determine the shape of the ordinate distribution and are sensitive to single extremes. The lowest value of the parameter S_{sk} = -2 and the highest value of kurtosis S_{ku} = 13.5 µm were recorded for the value AMo5_1. As shown in Fig. 14 a, this surface has the highest single vertices and many pits. High S_{ku} values of the surface of the Al_2O_3 coating indicate the surface geometry, which contains high, sharp peaks of the surface irregularities, which may be worn more intensively by the softer PEEK/BG material which results in a higher coefficient of friction. The negative skewness of the tested layers (parameter S_{sk} in Table 2), both before and after the tribological test, indicates the surfaces of all layers of a plateau character, which is well reflected in the isometric images - Figs. 10 to 14. The analysis of S_p and S_v or S_p and S_z parameters give information

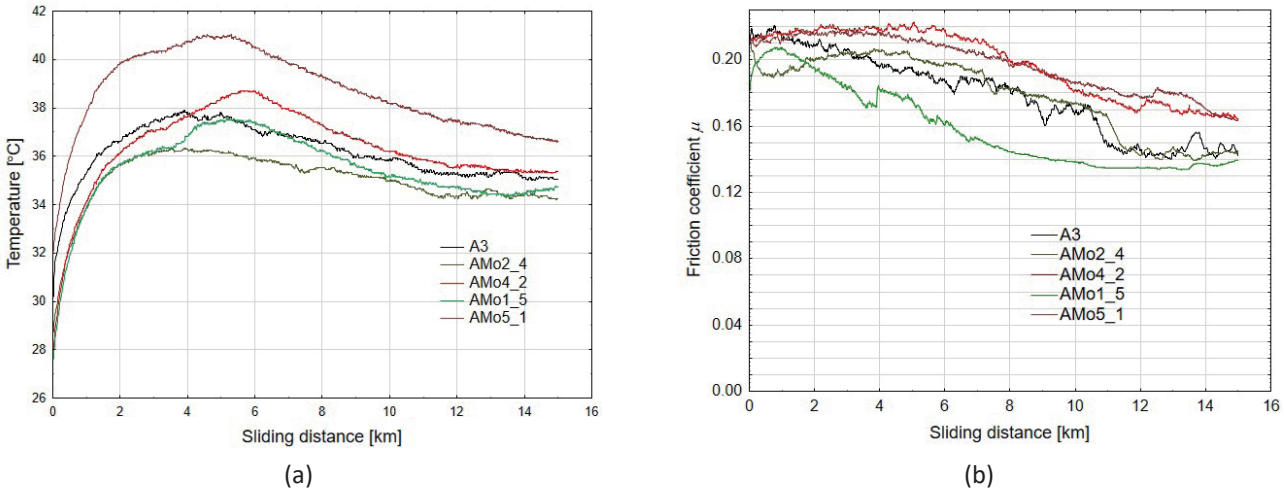

Fig. 8 The diagram of the temperature changes of PEEK/BG material (a) and of the friction coefficient (b) versus sliding time

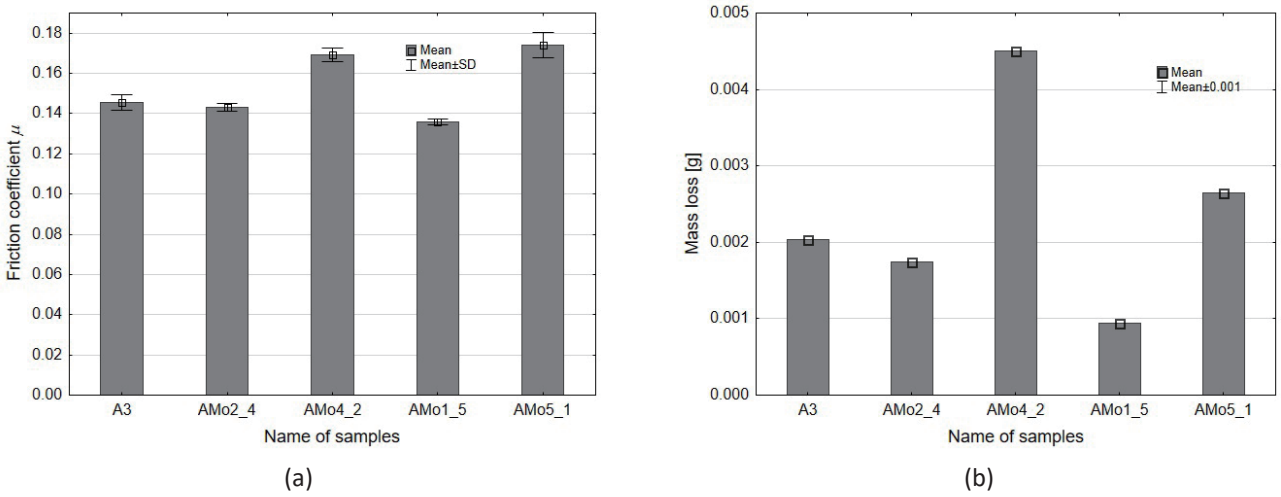

Fig. 9 The diagram of the average friction coefficient for each sample (a) and the value of the mass loss of PEEK/BG plastic for each sample (b)

profile shape and allows to conclude on the abrasion resistance of the tested surface. The A3 and AMo2_4 layers before tribological cooperation were characterized by the S_p / S_z << 0.5 ratio (Table 2), which suggests that the surface unevenness of these layers was characterized by vertex rounding (Figs. 10 a and 11 a), which increased their abrasion resistance. In the remaining layers before tribological cooperation, the ratio S_p / S_z > 0.5 (Table 2) indicates that their abrasion resistance was lower, mainly the AMo4_2 and AMo5_1 layers. After tribological cooperation, all layers were characterized by S_p / S_z << 0.5 (Table 2) and rounded vertices (Figs. 10 b - 14 b). According to the correlation analysis performed, it results that the parameters S_{ku} (Fig. 17 a) and S_q (Fig. 18 a) as well as the parameter S_p / S_z (Fig. 18 b) show a strong correlation with the friction coefficient μ. SGP assessment of the surface of the tested layers against friction, the values of tribological characteristics, and their

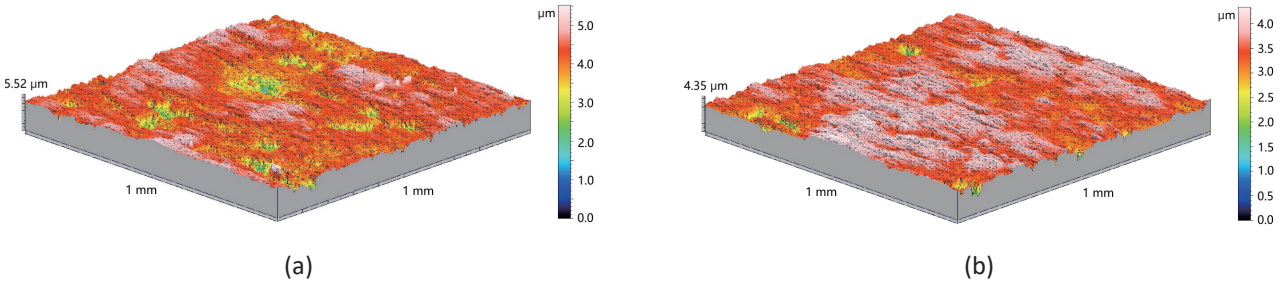

Fig. 10 Isometric images of A3 oxide layers before (a) and after (b) friction

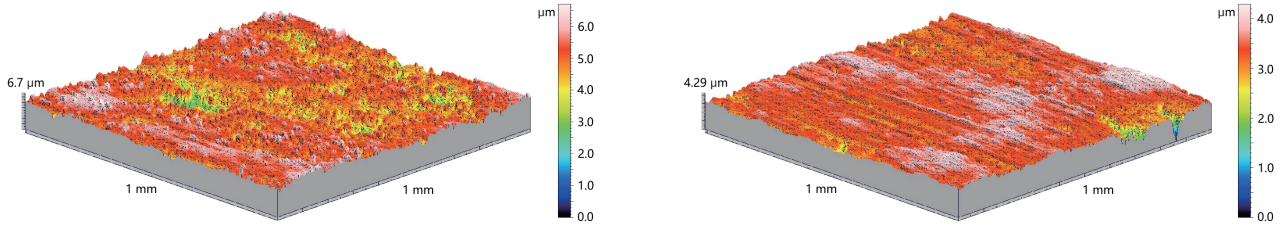

(a) (b)

Fig. 11 Isometric images of AMo2_4 oxide layers before (a) and after (b) friction

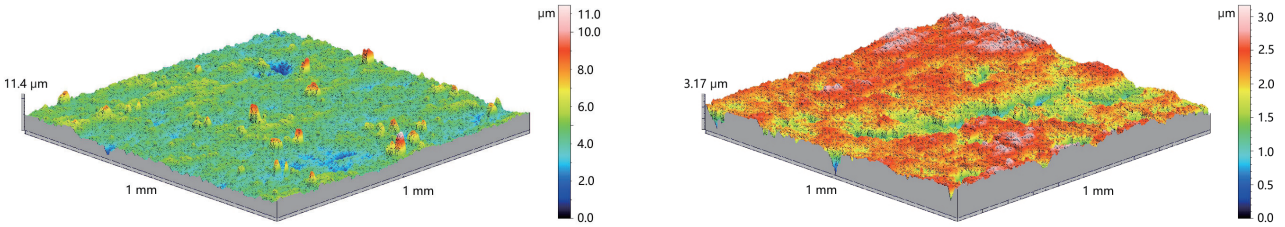

(a) (b)

Fig. 12 Isometric images of AMo4_2 oxide layers before (a) and after (b) friction

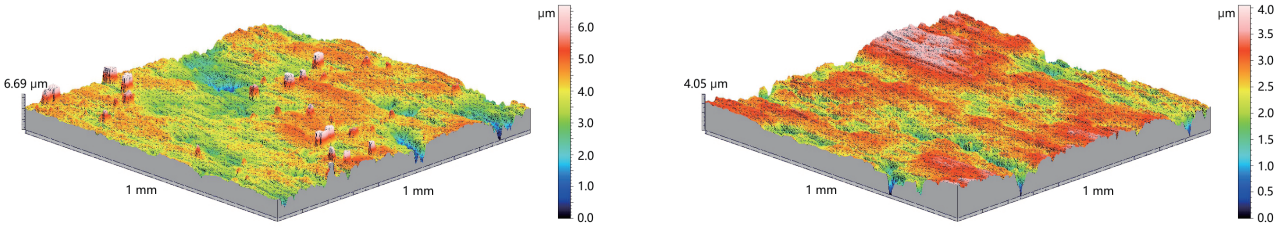

(a) (b)

Fig. 13 Isometric images of AMo1_5 oxide layers before (a) and after (b) friction

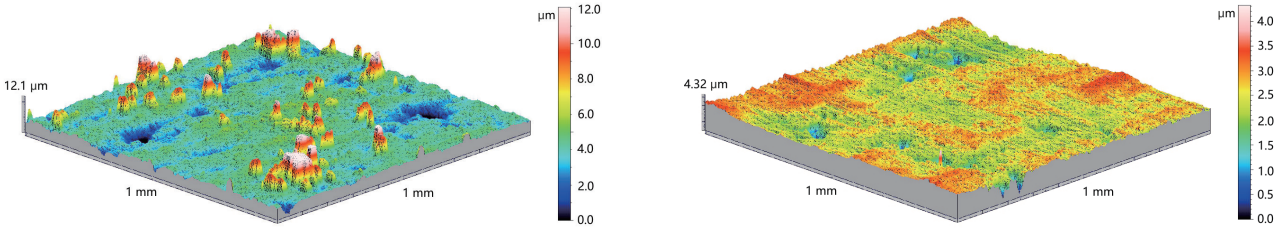

(a) (b)

Fig. 14 Isometric images of AMo5_1 oxide layers before (a) and after (b) friction

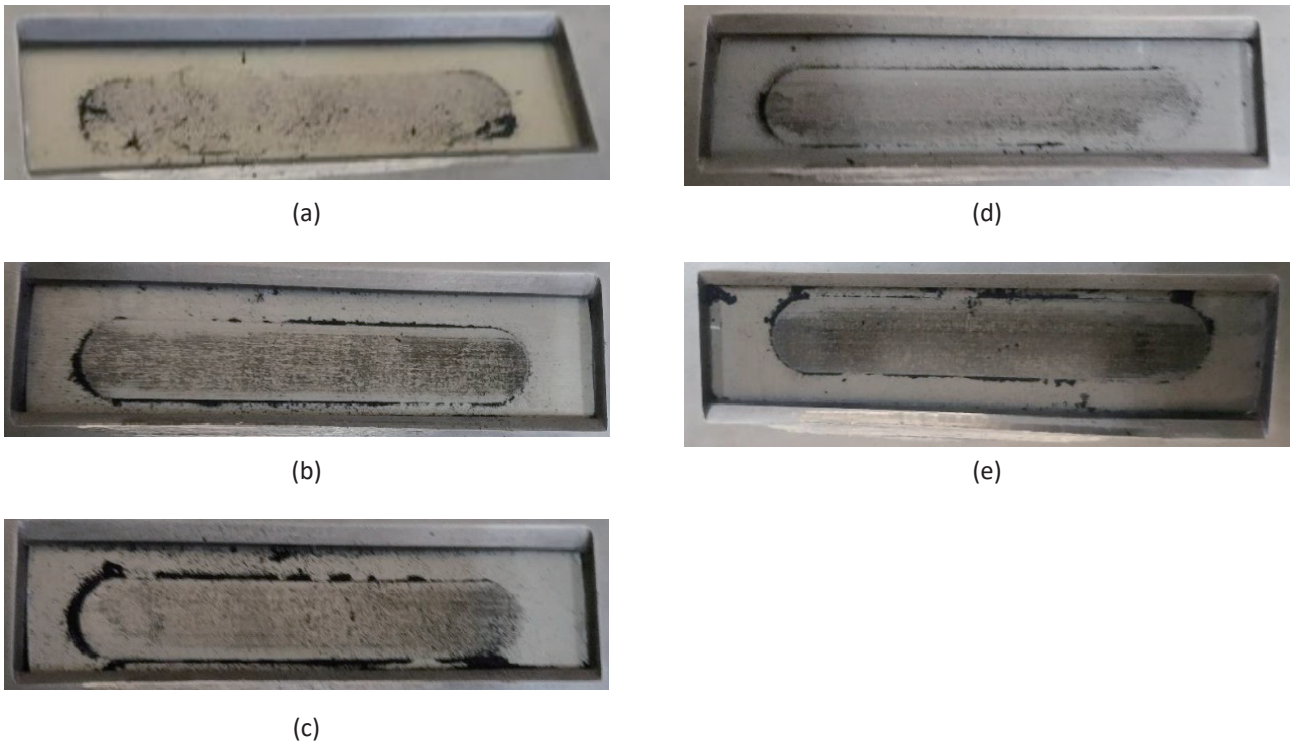

Fig. 15 Pictures of surface of (a) A3, (b) AMo2_4, (c) AMo4_2, (d) AMo1_5, (e) AMo5_1 sample after tribological test

Table 2 The amplitude parameters of the surface geometrical structure of counter-specimen before and after the tribological test for measured counter-specimen

Sample	**SGP parameters**							**SGP parameters**						
	S_q µm	S_{sk}	S_{ku}	S_p µm	S_v µm	S_z µm	S_p/S_z	S_q µm	S_{sk}	S_{ku}	S_p µm	S_v µm	S_z µm	S_p/S_z
	Before tribological test							After tribological test						
A3	0.672	-1.77	8.89	1.86	4.18	5.35	0.35	0.427	-2.84	18	0.784	3.44	3.91	0.2
AMo2_4	0.739	-0.242	6.02	1.82	3.28	5.03	0.36	0.387	-1.98	8.77	1.12	2.96	3.79	0.29
AMo4_2	0.809	-0.459	11.6	4.99	6.13	8.39	0.59	0.394	-1.27	6.38	0.912	2.11	2.92	0.31
AMo1_5	0.786	-0.91	5.96	2.86	3.3	5.47	0.52	0.527	-1.86	9.13	1.01	3.22	4.07	0.25
AMo5_1	1.37	-2	13.5	8.13	4.27	11.5	0.71	0.478	-2.44	13.4	0.976	3.3	4.03	0.24

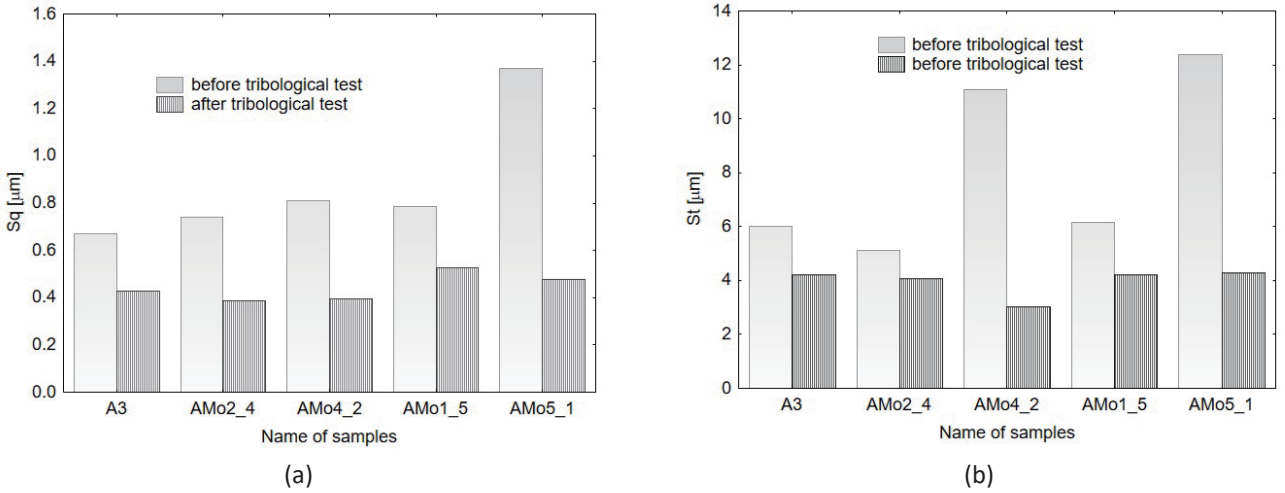

Fig. 16 Mean square profile deviation S_q (a) total depth of the S_t profile for individual surface layers (b) before and after the tribological test

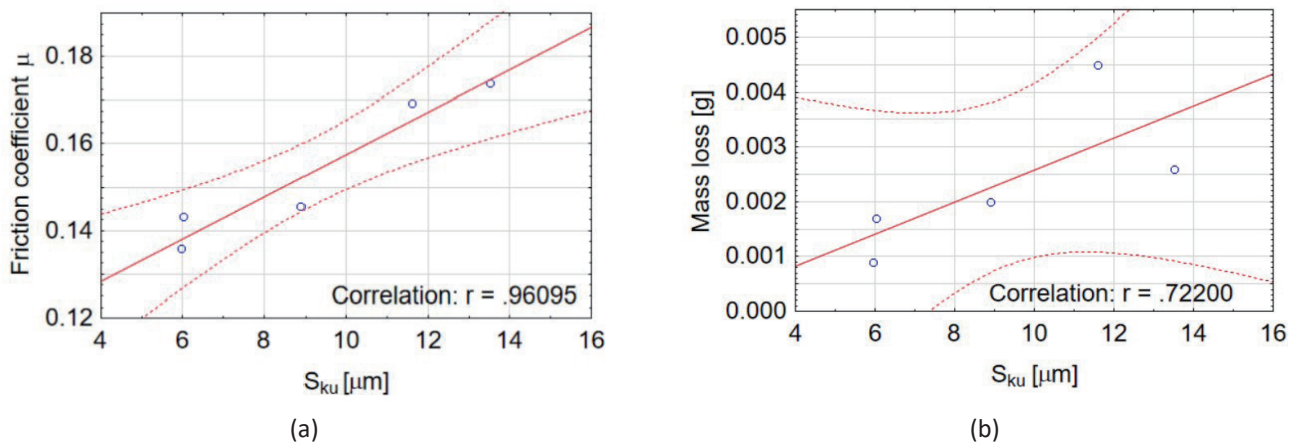

Fig. 17 Dependencies between (a) friction coefficient μ and S_{ku} parameter, (b) mass loss, and S_{ku} parameter

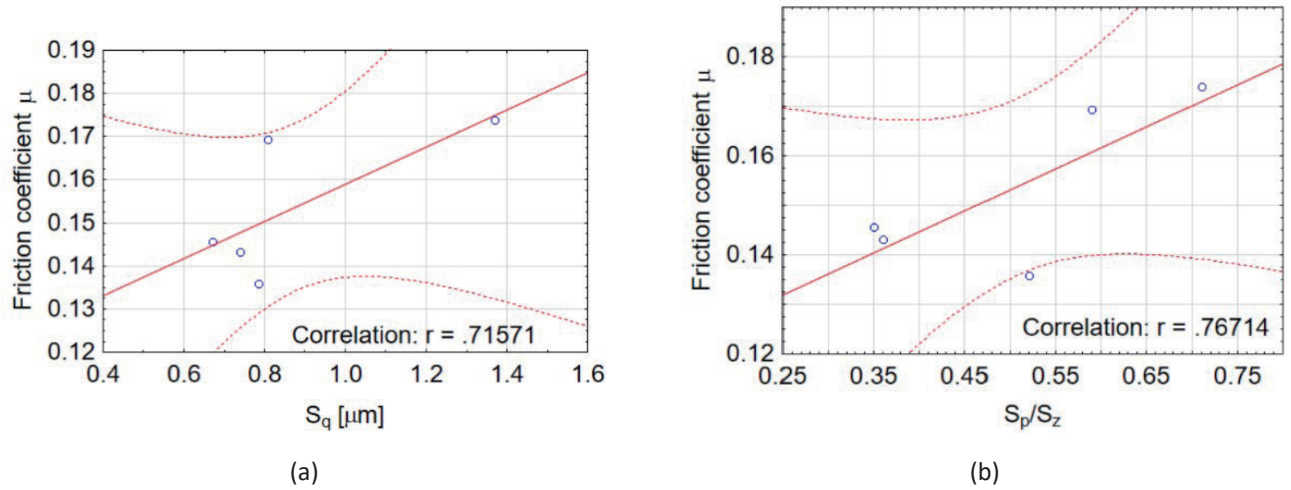

Fig. 18 Dependencies between (a) friction coefficient μ and S_q parameter, (b) friction coefficient μ, and S_p/S_z parameter

potential application can be predicted.

Table 3 presents the parameters of the Abbott-Firestone curve of the surface of the layers before and after the tribological test. The AMo5_1 layer showed the most significant differentiation to the S_{pk} parameter. This parameter is important in the running-in process. The S_k parameter describes the nominal surface roughness (roughness height of the core). Its values for the obtained layers were in the range of 1.19-1.82 μm before the test and 0.752-0.993 μm after the tribological test. The S_k parameter controls the tribological properties of workpieces during the steady-state period. As shown macroscopically in Fig. 15 d, the AMo1_5 layer was characterized by a small amount of PEEK/BG sliding film, the lowest coefficient of friction $\mu = 0.136 \pm 0.002$ (Figs. 8 b and 9 a) and the lowest PEEK/BG wear value of 0.0009 g. Our observations are consistent with the statement that friction variability results from the gradual change of liquid lubricant into the solid matter with decreasing film thickness [24, 25]. The highest S_k parameter also characterizes this layer after friction test equal to 0.993 mm. Looking at the S_{pk} parameter, which is important for the run-in period, it can be seen that its value

Table 3 The Abbott-Firestone curve parameters before and after tribological interaction for measured counter-specimen

Sample	S_k [μm]		S_{pk} [μm]		S_{vk} [μm]	
	before test	after test	before test	after test	before test	after test
A3	1.19	0.752	0.375	0.195	1.35	0.789
AMo2_4	1.54	0.755	0.56	0.325	1.3	0.633
AMo4_2	1.67	0.768	0.973	0.278	1.11	0.725
AMo1_5	1.56	0.993	0.724	0.223	1.28	1.01
AMo5_1	1.82	0.833	3.35	0.274	1.59	1.01

S_k – core roughness depth, S_{pk} – reduced peak height, S_{vk} – reduced valley depth

was particularly high at 3.35 μm for the AMo5_1 layer before the friction process. This layer was characterized by the highest coefficient of friction μ = 0. 174 ± 0.006 (Fig. 9 a) and the second-largest loss of the PEEK/BG polyμer (Fig. 9 b) with the value of 0.0026 g. The low value of the S_{pk} parameter indicates increased abrasion resistance. As shown in Table 3 and Fig. 19 b, the parameter S_{pk}, after tribological cooperation, takes comparable, relatively low values. This behavior means that after changing the nature of cooperation from lapping to the proper stage, all Al_2O_3 layers in terms of the geometry of the surface topography were resistant to abrasion thanks to the resulting layer of the PEEK/BG sliding film, which, as more plastic material, was subject to abrasion or adhesion to the layer surface. The S_{vk} parameter determines the ability to transfer the material to the oxide surface and keep it in the roughness cavities or is related to lack of lubrication. The highest value of the parameter S_{vk} = 1.59 μm before the tribological test had the AMo5_1 layer, which was characterized by a high coefficient of friction. The correlation analysis presented in Figs. 20 a and b shows a strong positive correlation between S_k and S_{pk}'s parameters and the friction coefficient μ. For the S_{vk} parameter, no strong correlation was observed between its value and the tribological properties of the sliding pair.

In the Fig. 21 the scheme of the difference in the running-in behavior between a gradient structure and a non-gradient structure was presented. The obtained results indicate that the application of high current densities at the beginning of the electrolytic coating production process leads to the production of non-gradient coatings with higher SGP amplitude parameters. This property translates directly into higher wear of the sliding PEEK/BG material and higher values of the friction coefficients of the tribological pairs thus obtained. Higher-amplitude surface irregularities intensify the wear of soft PEEK/BG during the lapping process.

5 Conclusion

The article presents the results of morphology, microstructure, stereometric and tribological properties of Al_2O_3 surface layers produced electrolytically by the alternating current method in the presence of molybdenum disulfide. The layers were designed with tribological applications in mind, which determine their application. To compare with referring sample obtained at the constant current method at 3 A/dm^2, the samples with the flowing current gradually increased or reduced to maintain an average current intensity of 3 A/dm^2

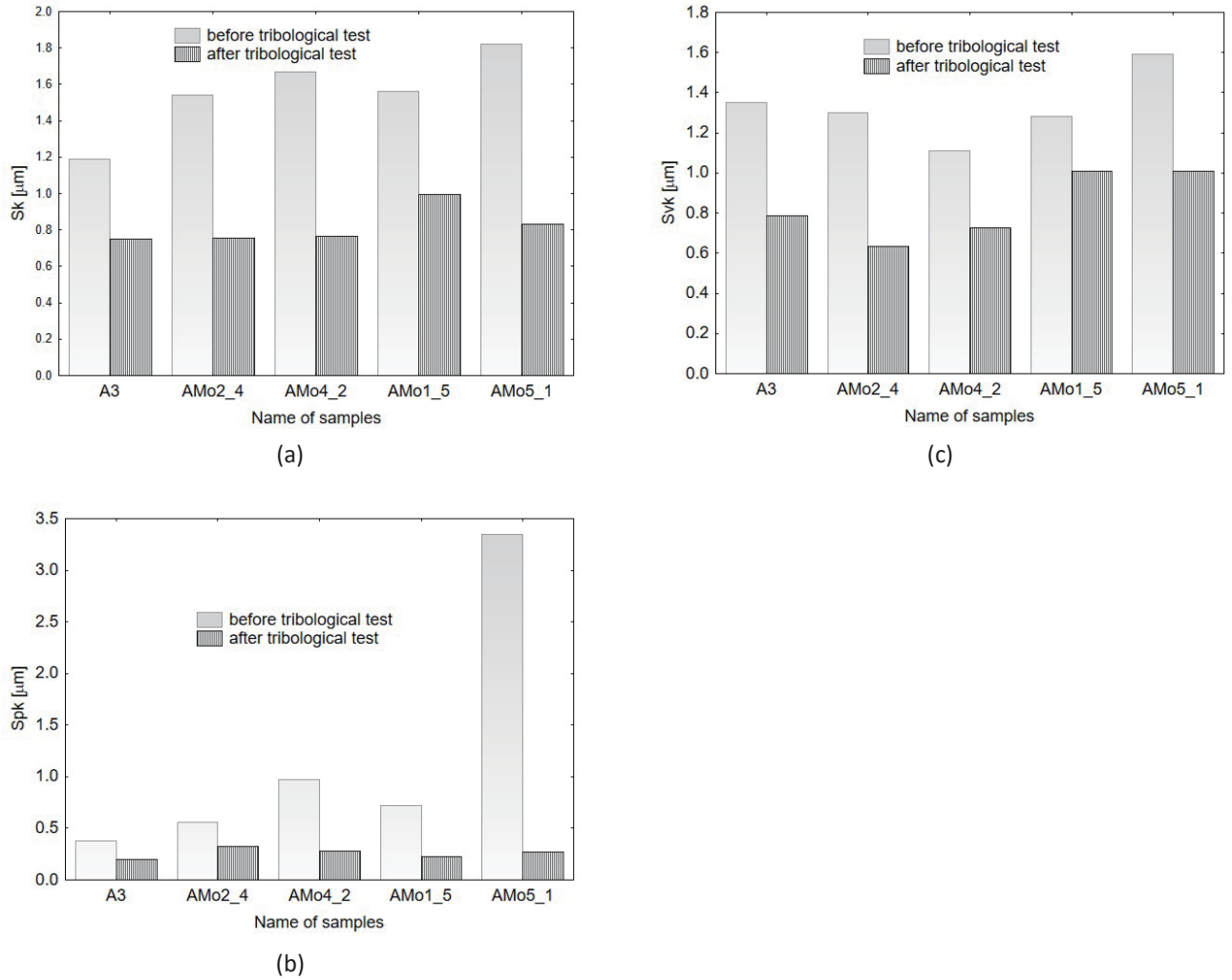

Fig. 19 Parameters of the Abbott-Firestone curve before and after tribological cooperation for the tested samples (a) S_k (core roughness depth), (b) S_{pk} (reduced peak height), and (c) S_{vk} (reduced valley depth)

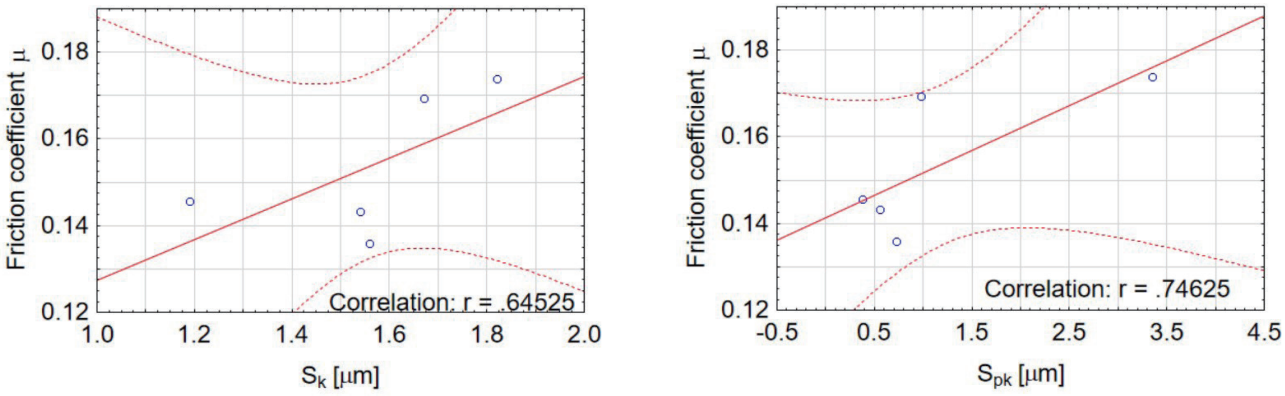

Fig. 20 Dependencies between (a) friction coefficient μ and S_k parameter, (b) friction coefficient μ and S_{pk} parameter

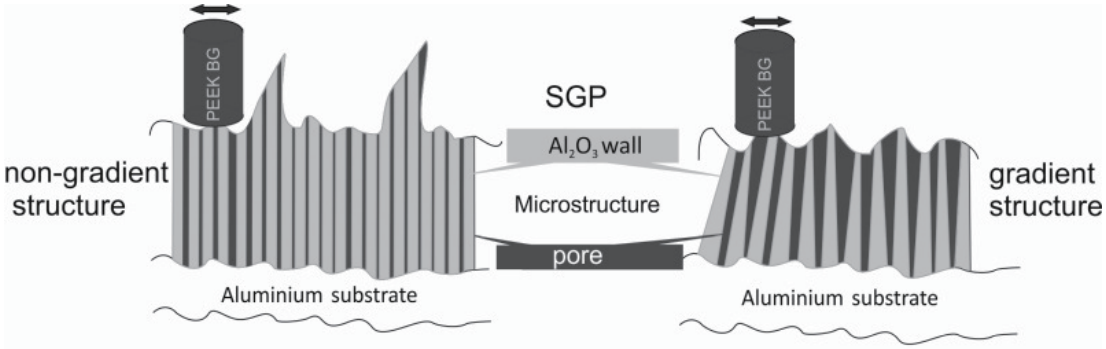

Fig. 21 Scheme of the difference in the running-in behavior between a gradient structure and a non-gradient structure

were prepared. As a result of the conducted experiments, it was possible to obtain a different character of the microstructure of aluminum oxide fibers in the produced layers.

The following conclusions were drawn from this research.

A greater change in the current density during the hard anodizing process reduces the thickness of the obtained surface layers.

The base sample A3 and samples AMo2_4 and AMo1_5 were characterized by a gradient fiber structure. In the case of AMo4_2 and AMo5_1, the layers were characterized by a constant value of the wall size of aluminum oxide fibers. The use of a higher current density at the beginning of the electrolytic coating process is associated with an increase in the thickness of the fibers and a decrease in porosity, which will lead to counteracting the natural process of the formation of a gradient structure change.

The lowest values of the coefficient of friction and weight loss of PEEK/BG material were recorded for samples obtained by gradually increasing non-periodic alternating current.

The gradient structure favors the reduction of the friction coefficient and weight loss of PEEK/BG in the tested friction pairs, and the application of the gradually increased non-periodic alternating current method improved the tribological properties compared to the base sample.

The method of gradually reducing non-periodic alternating current allowed to obtain a more homogeneous microstructure of aluminum oxide, but it deteriorated tribological properties compared to the base sample. The use of high current densities at the beginning of the process therefore leads to the production of non-gradient coatings characterized by higher SGP amplitude parameters.

Analyzes the correlation of S_{ku}, S_q, and S_p / S_z and the Abbott-Firestone curve S_k and S_{pk} parameters before the tribological cooperation of PEEK/BG pairs - Al_2O_3 oxide coating showed a strong correlation with the friction coefficient μ. Therefore based on the preliminary evaluation of SGP parameters of the surface of the tested layers against friction, the values of tribological characteristics of these pairs can be predicted.

Author Contributions: Conceptualization, J.K., T.K; sample preparation, A.K., M.K., tribology tests M.K., T.K., wall dimensions calculation A.K.; formal analysis, J.K., T.K.; SEM investigation D.B.; microhardness measurements, A.B.; writing—original draft preparation, J.K.; writing—review and editing, J.K.; visualization, J.K.. All the authors have read and agreed to the published version of the manuscript.

Funding: This research received no external funding.

Conflicts of Interest: The authors declare no conflict of interest.

References

[1] Niedźwiedź, M., Skoneczny, W. and Bara, M., "The Influence of Anodic Alumina Coating Nanostructure Produced on EN AW-5251 Alloy on Type of Tribological Wear Process," Coatings, 10, 2, 2020, 105.

[2] Niedźwiedź, M., Skoneczny, W. and Bara, M., "Influence of Conditions for Production and Thermo-Chemical Treatment of

Al_2O_3 Coatings on Wettability and Energy State of Their Surface," Coatings, 10, 7, 2020, 681.

[3] Kwolek, P., "Hard Anodic Coatings on Aluminum Alloys," Advances in Manufacturing Science and Technology, 41, 3, 2017, 35-46.

[4] Bruera, F. A., Kramer, G. R., Vera, L. and Ares, A. E., "Low-Cost Nanostructured Coating of Anodic Aluminium Oxide Synthesized in Sulphuric Acid as Electrolyte," Coatings, 11, 3, 2021, 309.

[5] Michalska-Domańska, M., Stępniowski, W. J. and Salerno, M., "Effect of Inter-Electrode Separation in the Fabrication of Nanoporous Alumina by Anodization," Journal of Electroanalytical Chemistry, 823, 2018, 47-53.

[6] Chowdhury, P., Thomas, A. N., Sharma, M. and Barshilia, H. C., "An Approach for *In Situ* Measurement of Anode Temperature during the Growth of Self-Ordered Nanoporous Anodic Alumina Thin Films: Influence of Joule Heating on Pore Microstructure," Electrochimica Acta, 115, 2014, 657-664.

[7] Lämmel, C., Schneider, M., Heubner, C., Beckert, W. and Michaelis, A., "Investigations of Burning Phenomena during the Hard Anodising of Aluminium by Local *In-Operando* Temperature Measurements," Electrochimica Acta, 249, 2017, 271-277.

[8] Chi, C. S., Lee, J. H., Kim, I. and Oh, H. J., "Effects of Microstructure of Aluminum Substrate on Ordered Nanopore Arrays in Anodic Alumina," Journal of Materials Science & Technology, 31, 7, 2015, 751-758.

[9] Lee, W., Schwirn, K., Steinhart, M., Pippel, E., Scholz, R. and Gösele, U., "Structural Engineering of Nanoporous Anodic Aluminium Oxide by Pulse Anodization of Aluminium," Nature Nanotechnology, 3, 4, 2008, 234-239.

[10] Mohammadi, I. and Afshar, A., "Modification of Nanostructured Anodized Aluminum Coatings by Pulse Current Mode," Surface and Coatings Technology, 278, 2015, 48-55.

[11] Kwolek, P., Drapała, D., Krupa, K., Obłój, A., Tokarski, T. and Sieniawski, J., "Mechanical Properties of a Pulsed Anodised 5005 Aluminium Alloy," Surface and Coatings Technology, 383, 2020, 125233.

[12] Fratila-Apachitei, L. E., Duszczyk, J. and Katgerman, L., "AlSi(Cu) Anodic Oxide Layers Formed in H_2SO_4 at Low Temperature Using Different Current Waveforms," Surface and Coatings Technology, 165, 3, 2003, 232-240.

[13] Shih, H. H. and Tzou, S. L., "Study of Anodic Oxidation of Aluminum in Mixed Acid Using a Pulsed Current," Surface and Coatings Technology, 124, 2-3, 2000, 278-285.

[14] Ashassi-Sorkhabi, H., Hagrah, A., Parvini-Ahmadi, N. and Manzoori, J., "Zinc-Nickel Alloy Coatings Electrodeposited from a Chloride Bath Using Direct and Pulse Current," Surface and Coatings Technology, 140, 3, 2001, 278-283.

[15] Roshani, M., Rouhaghdam, A. S., Aliofkhazraei, M. and Astaraee, A. H., "Optimization of Mechanical Properties for Pulsed Anodizing of Aluminum," Surface and Coatings Technology, 310, 2017, 17-24.

[16] Chung, C. K., Liao, M. W., Lee, C. T. and Chang, H. C., "Anodization of Nanoporous Alumina on Impurity-Induced Hemisphere Curved Surface of Aluminum at Room Temperature," Nanoscale Research Letters, 6, 2011, 596.

[17] Dzierwa, A., "Influence of Surface Preparation on Surface Topography and Tribological Behaviours," Archives of Civil and Mechanical Engineering, 17, 3, 2017, 502-510.

[18] Pawlus, P. and Dzierwa, A., "Tribological Behavior of Functional Surface: Models and Methods," Coatings, 11, 3, 2021, 1-3.

[19] Miller, T., Adamczak, S., Świderski, J., Wieczorowski, M., Łetocha, A. and Gapiński, B., "Influence of Temperature Gradient on Surface Texture Measurements with the Use of Profilometry," Bulletin of the Polish Academy of Sciences: Technical Sciences, 65, 1, 2017, 53-61.

[20] Radek, N., Pietraszek, J., Gadek-Moszczak, A., Orman, Ł. J. and Szczotok, A., "The Morphology and Mechanical Properties of ESD Coatings before and after Laser Beam Machining," Materials (Basel), 13, 10, 2020, 2331.

[21] Johansson, S., Nilsson, P. H., Ohlsson, R., Anderberg, C. and Rosén, B. G., "New Cylinder Liner Surfaces for Low Oil Consumption," Tribology International, 41, 9-10, 2008, 854-859.

[22] Menezes, P. L., Kishore, K. J., Kailas, S. V. and Lovell, M. R., "Friction and Transfer Layer Formation in Polymer-Steel Tribo-System: Role of Surface Texture and Roughness Parameters," Wear, 271, 9-10, 2011, 2213-2221.

[23] Singh, J. and Chauhan, A., "A Review on Sliding Wear Behaviour of Aluminium Matrix Composites with Hybrid Reinforcements for Automotive Applications," Tribology Online, 9, 3, 2014, 121-134.

[24] Wang, S., Hu, Y. Z., Wang, W. Z. and Wang, H., "Transition of Frictional States and Surface Roughness Effects in Lubricated Contacts," Proceedings of the Institution of Mechanical Engineers, Part J: Journal of Engineering Tribology, 222, 3, 2008, 407-414.

[25] Wang, S., Hu, Y. Z. and Tan, Q. C., "Frictional Behaviour of Engineering Surfaces in Overall Lubrication Regimes of Point Contacts," Proceedings of the Institution of Mechanical Engineers, Part J: Journal of Engineering Tribology, 225, 11, 2011, 1071-1080.

[26] Kubiak, K. J., Liskiewicz, T. W. and Mathia, T. G., "Surface Morphology in Engineering Applications: Influence of Roughness on Sliding and Wear in Dry Fretting," Tribology International, 44, 11, 2011, 1427-1432.

[27] Sedlaček, M., Podgornik, B. and Vižintin, J., "Influence of Surface Preparation on Roughness Parameters, Friction and Wear," Wear, 266, 3-4, 2009, 482-487.

[28] Sedlaček, M., Podgornik, B. and Vižintin, J., "Correlation between Standard Roughness Parameters Skewness and Kurtosis and Tribological Behaviour of Contact Surfaces," Tribology International, 48, 2012, 102-112.

[29] Korzekwa, J., Bara, M. and Karpisz, D., "Sample Preparation Methodology of the Al_2O_3 Surface Layers for Self-Lubricating Sliding Pair," In: WCCM-ECCOMAS2020, 2020, 1-11.

[30] Dzierwa, A., Pawlus P. and Zelasko, W., "The Influence of Disc Surface Topography after Vapor Blasting on Wear of Sliding Pairs under Dry Sliding Conditions," Coatings, 10, 2, 2020, 102.